Design of Circularly Polarized and Highly Depointing Reflectarrays with high polarization purity

Andrea Guarriello, Daniele Bresciani, Hervé Legay, George Goussetis, Renaud Loison

Design of Circularly Polarized and Highly Depointing Reflectarrays with high polarization purity

Andrea Guarriello* †, Daniele Bresciani‡, Hervé Legay‡, George Goussetis† Renaud Loison*
*IETR, National Institute of Applied Sciences, Rennes, France, Andrea.Guarriello@insa-rennes.fr
†Institute of Sensors, Signals and Systems, Heriot-Watt University, Edinburgh, United Kingdom
‡Direction of Research, Thales Alenia Space, France

***Abstract*—This work aims to investigate the limitations and possible solutions in designing highly tilted radiation pattern reflectarrays working in double circular polarization and fed by an onset single primary source. To this extent, three single-layer monolithic reflectarrays, producing a pencil beam at increasing radiation angles with high X-polarization discrimination (XPD) have been designed and analyzed. A direct optimization technique shows that an XPD=20 dB can be attained for radiation patterns pointing at sixty degrees, at the cost of co-polarised directivity degradation. An analysis of the target aperture fields, obtained through backscattering techniques, shows that an amplitude modulation on the aperture field components is necessary to obtain highly tilted radiation patterns with high XPD. Since reflectarray cells are not able to produce such amplitude components unbalance, an elliptically polarized source is considered, producing an incident field components amplitude unbalance that results in a radical reduction of the X-polarization levels.**

***Index Terms*—reflectarray, optimization, circular polarization, tilted beam.**

I. Introduction

High-gain antennas, which produce narrow beams with elevated gain values able to support high data rate capabilities demanded in space telecommunications, are essential in many applications, spanning telecom space missions, scientific space missions, radars, and long-distance communications. High-gain antennas traditionally employed in the space sector rely on metallic parabolic or shaped reflectors and antenna arrays. Beyond several advantages, both systems suffer from some limitations related to the antenna volume, cost, mass, and efficiency, which are of capital importance for antenna integration in the spacecraft system.

Reflectarray antennas (RAs) are an alternative technology able to alleviate most of the limitations described above while benefiting from the advantages of the conventional reflectors and array antennas for high gain applications [1].

For space application, dual circularly polarized RAs are of high interest due to their several advantages. They allow an increment of the communication link capability by using the two different right hand (RH) and left hand (LH) circular polarization (CP), enabling two different communication channels. Moreover, CP is less sensitive to interference and multi-path losses than linear polarization, and it is less affected by atmospheric and ionospheric losses. The use of two orthogonal CP components demands high polarization discrimination (XPD) between the RHCP and LHCP.

Tilted RAs at high radiation angles can find applications in missions requiring object tracking through radar systems or missions requiring to direct the beam toward off-nadir ground stations. It is frequent, especially in low Earth orbit applications, where the satellites are often in ground station visibility at low elevation angles.

In this paper, the issue of designing highly depointing dual-CP RA is addressed. The main objective consists in analyzing the reasons for the intrinsic difficulties in obtaining depointing radiation patterns with high cross-polarization discrimination. The problem analysis can be exploited to find efficient solutions for the design of tilted beam or broad beam RAs.

Highly tilted RA has been addressed in several works, but few references highlight the dual-polarization capabilities. In [2] and [3], the feed displacement technique is adopted in order to achieve respectively $\pm 30^\circ$ and $\pm 45^\circ$ scanning ranges, without addressing the issue of double circular polarization use. In [4] a scanning angular range of $\pm 70^\circ$ is successfully achieved through combined feed and RA rotation, at the cost of 3.7 dB scan losses. Once again, the dual-polarization issue is not addressed in this work. Another work [5] deals with the scanning capabilities of mechanically reconfigurable elements RA antennas, showing a visible degradation of the polarization purity as the scanning angle increases. The scanning losses are evaluated at 3.7 dB for a scanning range of $\pm 60^\circ$, while the X-polarization increases drastically from 20° and above. In [6] a 60 GHz electronically reconfigurable RA for imaging systems is presented. With scanning capabilities over a $\pm 25^\circ$ range, it presents XPD levels that are excellent for beams scanned at the azimuth angle of 0°, while those at the azimuth angle of 20° are degraded by up to 22 dB.

This paper shows and discusses the issues of X-polarization discrimination for highly depointing passive RAs. In the first instance, three different onset single-feed RAs, with the same geometrical features and in the same configuration, are designed and optimized for beam pointing angles of $\theta_1 = 0^\circ$, $\theta_2 = 30^\circ$ and $\theta_3 = 60^\circ$. The design and optimization methodology are briefly presented.

Subsequently, the target aperture field analysis is performed through advanced analysis methodologies, notably backscatter-

ing techniques. This second step allows to identify the requirements needed to design low X-polarization highly depointing RA and helps to highlight the reasons for the difficulties when dealing with flat apertures passive antennas.

II. Analysis and design of tilted pencil beam RA

A. RA features

1) RA geometry: The RA (Fig. 1) comprises a single layer monolithic panel fed by a conventional onset horn working in the frequency band $f = [25.5; 27.00]$ GHz with a center frequency of 26.25 GHz. The RA is circular with a diameter fixed to 300 mm, corresponding to roughly 26.3λ (λ the free-space wavelength at the center frequency). In this work, the bandwidth issue is not addressed, so only the central frequency is considered in the following.

The feeder illuminates the RA panel with an onset-centered configuration with $f/D = 0.52$. The feed illuminates in *RHCP* and *LHCP* with a taper of $11.5\,dB$ at $\theta^{inc} = 45°$. The RA parameters are summarized in Table I referring to the coordinate system and definitions shown in Figure 1.

TABLE I
RA features

RA geometry	circular
Dimensions	$D_x = D_y = 300$ mm
Unit cell lattice	$p_x = p_y = 3.80$ mm
Number of cells	4899
Substrate thickness	$t = 1.524$ mm
Substrate permettivity	$\varepsilon_r = 3.55$
Loss tangent	$\tan\delta = 0.0027$
Focal distance	$f = 156.7$ mm
Feed offset angle	$\theta^f = 0°$

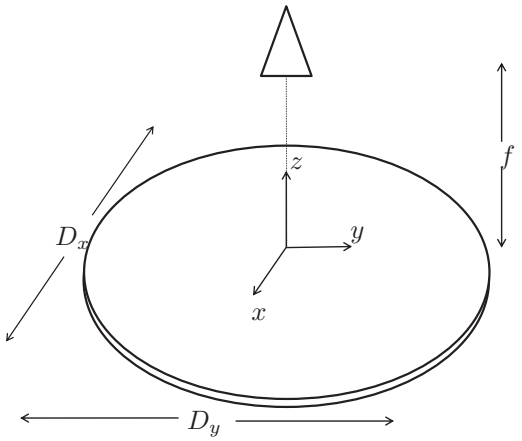

Fig. 1. RA antenna geometry

2) Array constitutive elements and 1D look-up table handling: As array elements, the first and second-order Phoenix cells [7], [8] are selected. The square patch/slot loop periodic cycle on the bottom of figure 2 is considered. This cycle avoids sharp geometrical transitions for adjacent cells, and it is composed of first and second-order inductive Phoenix cells. Figure 2 shows the behavior of the cells as a function of the auxiliary periodic variable ξ defined as:

$$\xi(d_1, d_2) = \begin{cases} \dfrac{d_1 - d_{1_{max}}}{d_{1_{max}} - d_{1_{min}}}\pi & \text{, if } d_2 = 0 \\ \dfrac{d_2 - d_{2_{min}}}{d_{2_{max}} - d_{2_{min}}}\pi & \text{, if } d_1 = d_{1_{max}} \end{cases} \quad (1)$$

where d_1, d_2 are shown in the inset of figure 2. The geometrical parameters are set according to standard fabrication tolerances, $toll = 0.1$ mm. Therefore, the geometrical parameters are set to $d_{1_{min}} = 0.1$ mm, $d_{1_{max}} = 3.7$ mm, $d_{2_{min}} = 0.1$ mm and $d_{2_{max}} = 3.5$ mm. In figure 2, the reflection phase is calculated under normal plane wave incidence and displayed as a function of ξ. The lookup table is computed for all the incidences relative to the RA geometry as seen from the feed. The cells characterization is performed though periodic surface analysis program based on the Floquet expansion of the unit cell scattered field, derived through the Method of Moments. The local periodicity of the RA layout must be therefore respected.

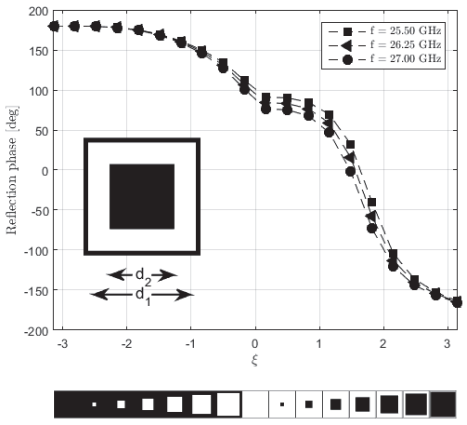

Fig. 2. Phase of the scattering coefficient of a square loop/slot combination element in a periodic environment as function of the periodic parameter ξ describing the geometry. In the inset the relevant parameters defining the cell's geometry.

The variation of the phase curves shows that an almost complete 360° phase cycle is achieved, with a phase gap of $\approx 15°$, considered as acceptable.

B. Design through aperture field phase and far-field amplitude optimization

1) Co-polarization optimization: The preliminary layout design is performed with a classical phase only (PO) synthesis. The layout obtained is used as first guess solution for the next step that consists in minimizing the quadratic error on the aperture field components phase through a multiobjective optimization of the RA aperture field phase distribution, namely the aperture field optimization (AFO). It is done by describing the RA preliminary geometry distribution (obtained with

the PO synthesis) through the auxiliary periodic parameter ξ and representing the unwrapped ξ distribution through a continuous splines surface. This representation allows avoiding sharp geometrical transition among contiguous RA elements, thus respecting the quasi-periodic assumption made in the lookup table cells characterization. The results of the phase-only optimization are presented in figure 3. The radiation pattern is computed through the aforementioned Floquet's mode matching software and a Physical Optics software.

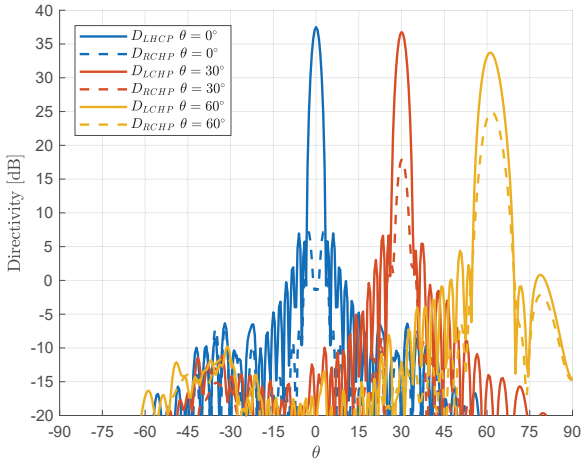

Fig. 3. Radiation pattern of the RAs obtained through aperture field optimization (AFO).

We can notice from figure 3 that the three RAs radiation pattern show a notable increment of the X-polarization levels as the beam tilting angle increases. To this extent, the RA radiating at broadside (specular direction of the incident field) shows high level of X-polarization discrimination of 38.65 dB. As the beam tilting angle increases, the X-polarization discriminantion deteriorate, by reaching 21.73 dB for the RA pointing at $\theta = 30°$ and a very low XPD for the RA in the tilting angle configuration $\theta = 60°$, with an XPD of 8.85 dB.

2) X-polarization optimization: The elementary cell considered for the single circular polarization design is described through one degree of freedom. By considering rectangular elements, it is possible to control the impinging wave delay and depolarize it slightly [9].

A direct optimization [10] with respect to a mask for the *RHCP* and *LHCP* is performed, namely the far-field amplitude optimization (FFO). This time, the objective is to minimize the maximum error between the radiation pattern and the prescribed mask by distorting the square cells geometry into rectangles ($d_x \neq d_y$) at global level, i.e. by guaranteeing the local periodicity assumption through splines projection of the parametrized layout and by keeping the original cells square lattice. More in detail, for each of the three cases, the RA layout is described through a continuous and derivable spline projection of the parameter ξ, identifying the cell index in the lookup table according to equations 1, and a cells distortion index h. The optimization variables are therefore the spline coefficients of the two surfaces Ξ and H describing the parametrized cells distribution. A *minimax* algorithm allows to minimize the maximum of the vectorial cost function described as the error on the radiation pattern amplitude with respect to the mask and the maximization of the XPD levels.

The initial condition is the single polarization design of section II-B1. The optimization is performed at the center frequency $f_0 = 26.25$ GHz for each of the three RA.

By looking at the plots of figure 4, we can notice that the XPD levels are kept well above 20 dB for the three RAs.

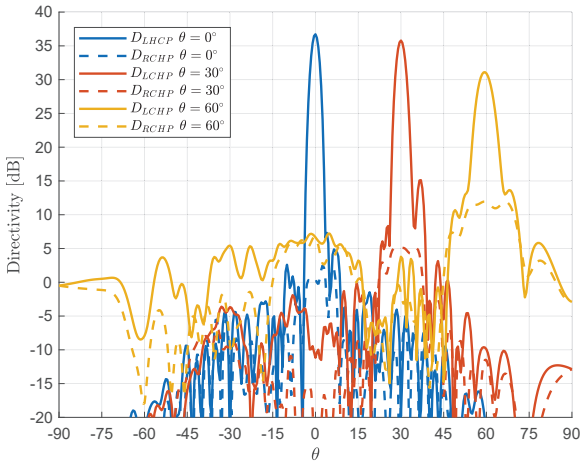

Fig. 4. Radiation pattern of the RAs obtained through far-field optimization (FFO).

The levels of X-polarization for the case $\theta_1 = 0°$ and $\theta_2 = 30°$ are reduced below -30 dB by preserving low levels of side lobes. The case $\theta_3 = 60°$ shows difficulties to increase the XPD levels above 20 dB. Moreover, we can see the apparition of an important radiation in the angular range $\theta \in [-30°; 20°]$. These results show that the reduction of the X-polarization levels obtained through the far-field direct optimization is generally accompanied by a degradation of the maximum levels of directivity. The co-polarization levels degradation is more accentuated as the beam tilting angle increases.

III. Aperture field reconstruction through X-polarization cancellation

Backscattering techniques [11] are adopted to obtain a RA ideal aperture field that allows obtaining a far-field with low X-polarization levels by keeping adequate co-polarization levels. It consists of enforcing the amplitude of the far-field X-polarization to be canceled for both *RHCP* and *LHCP* polarisation, and then derive the aperture field and the 2×2 reflection matrices of the RA elements that are the ideal reflection matrices to be realized.

The aperture field reconstruction is derived from the $\theta_3 = 60°$ radiation pattern of figure 3 with the X-polarization

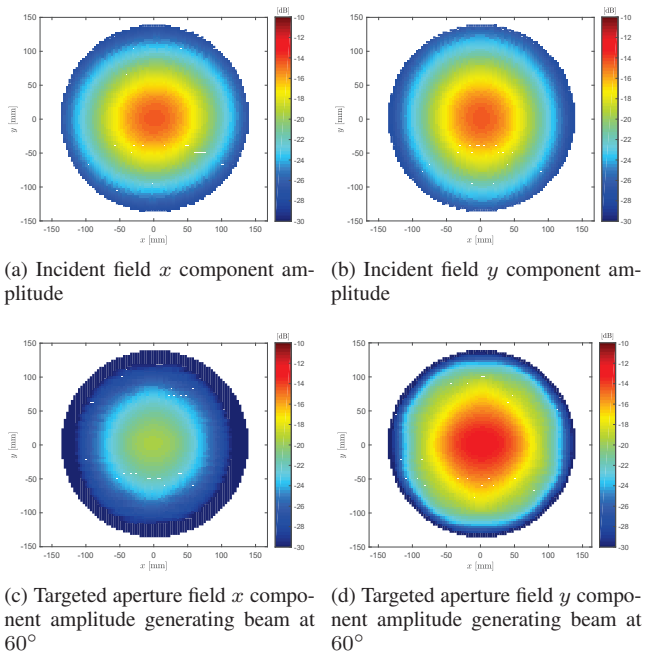

(a) Incident field x component amplitude

(b) Incident field y component amplitude

(c) Targeted aperture field x component amplitude generating beam at $60°$

(d) Targeted aperture field y component amplitude generating beam at $60°$

Fig. 5. Field amplitude distribution on the RA surface.

component forced to be null everywhere. Figures 5a and 5b map the amplitude of the incident field Cartesian components while figures 5c and 5d show the amplitude of the aperture field components obtained through backscattering technique.

As we may notice, the amplitude of the target aperture field is not realizable through a phase-only synthesis. The targeted RA aperture field has an amplitude higher or lower compared to the incident field. We can expect that RA cells cannot realize such an aperture field since the reflection matrix direct coefficients cannot have an amplitude greater than 0 dB. For a more exhaustive analysis, the comparison of the incident field components and the targeted aperture field components for the three reflectarray is shown in figure 6. We see that x and y components umbalance to achieve low X-polarization radiation pattern become more and more accentuated as the beam tilting angle increases. This explains why as the beam tilting angle increase, the realizable XPD degrades.

Examples of aperture field amplitude control can be found in literature in the context of broad-beam antennas, i.e., radiating at a highly tilted direction. In [12] the antenna aperture amplitude is locally controlled through parasitic elements to mitigate the X-polarization levels at high radiation angles. In [13] the amplitude of the aperture field is managed by controlling the leakage parameter of the metasurface elements. It allows a modulation of the aperture field amplitude to compensate for the polarization losses at high pointing radiation angles θ. From the other references in the literature (for instance [14], [15], [16]), we can find consistency with the latter explanation since the amplitude of the aperture field is not controlled, the broad-beam antennas suffer from high X-pol levels for radiation angles above $40°$.

As show in the previous section, even if a passive RA element cannot efficiently control the amplitude levels of the aperture field, a direct optimization in which the RA square patches and slots are deformed into rectangles can allow phase or amplitude compensation that at a global level can enhance the XPD levels at high radiation angles, at cost of a co-polarization deterioration.

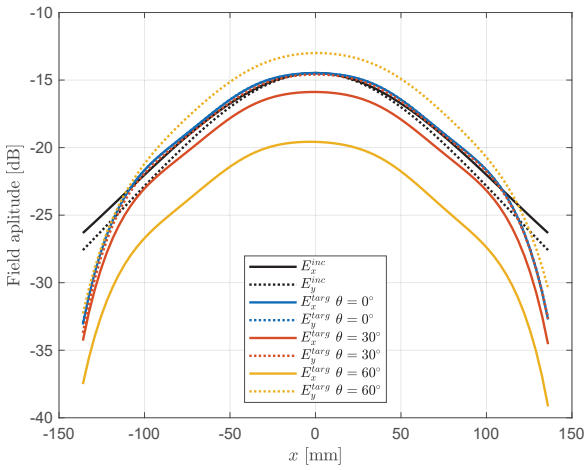

Fig. 6. Comparison of the incident field components and the targeted aperture field components $E_{x,y}^{targ}$ for the three reflectarray generating tilted beams with low X-polarization. Cut along $y = 0$.

IV. Reflectarray fed by an elliptically polarized source

The analysis of the target aperture field derived through backscattering techniques revealed that an amplitude unbalance between the components of the aperture field is necessary to obtain RA radiating low X-polarization at highly tilted angles. In this section, we explore an alternative feed design able to produce an incident field amplitude on the RA close to the one of figures 5c and 5d. The case RA radiating at $60°$ is considered, for the other cases the process is equivalent. The incident field amplitude unbalance means that the feed should radiate with highly elliptical polarization, with field components in phase quadrature and the amplitude of the components unbalanced according to the amplitude of the target aperture field components. This is obtained by exciting each of the two feed ports with a different normalized weight w_x and w_y.

A RA fed by the new primary source is designed, the layout is derived through AFO. Figure 7 shows the comparison of the three different designs of a RA radiating at $\theta = 60°$. In the present case the excitation weights are given by the amplitude relative unbalance of the target aperture field x and y components, $w_x \approx 0.89$ and $w_y \approx 0.45$. We can notice how the XPD levels have been enhanced drastically in the new design, reaching values superior to 40 dB. The beam tilting operated by the flat surface RA allows circularizing the

elliptical polarization components coming from the feed at the radiation angle direction 60°, greatly enhancing the circular polarization purity of the radiation pattern.

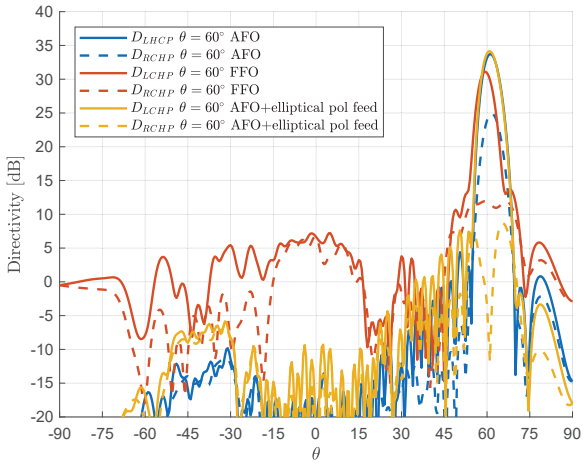

Fig. 7. Comparison of the radiation patterns for RA depointing at 60° obtained through aperture field phase optimization (blue), far-field direct optimization (red), aperture field phase optimization and RA illuminated by an elliptically polarized source (yellow).

V. Conclusion

Pencil beam RAs with various beam tilting angles have been analyzed and designed. The reduction of the X-polarization levels was confirmed to be challenging for RA radiating at highly tilted angles. Substantial improvements on the XPD levels can be achieved for each case surveyed through a direct optimization technique, at the cost of an increasing degradation on the co-polarization levels as the beam tilting angle increases. This study confirmed the impact of the limitations of passive RA cells to modulate the aperture field amplitude, which is necessary to achieve high X-polarization discrimination at highly tilted radiating angles. A solution to overcome the limitations on amplitude modulation imposed on passive reflectarray cells is to shape the incident field components coming from the primary source by balancing the source components excitation. To obtain a highly tilted beam radiation pattern with high circular polarization purity, a highly elliptically polarized feed should be designed. A radical improvement of the XPD$>$ 40 dB has been observed in the RA fed by an elliptically polarized source and radiating at $\theta = 60°$. The recommended ellipticity rate of the onset source polarization is more accentuated as the target beam tilting angle increases.

Acknowledgment

This work was supported by the European Commission under H2020 project REVOLVE (MSCA-ITN-2016-722840).

References

[1] J. Huang and J. A. Encinar. *Reflectarray Antenna*. John wiley & sons, 2008.

[2] Payam Nayeri, Fan Yang, and Atef Z. Elsherbeni. Bifocal design and aperture phase optimizations of reflectarray antennas for wide-angle beam scanning performance. *IEEE Transactions on Antennas and Propagation*, 61(9):4588–4597, 2013.

[3] Geng-Bo Wu, Shi-Wei Qu, and Shiwen Yang. Wide-angle beam-scanning reflectarray with mechanical steering. *IEEE Transactions on Antennas and Propagation*, 66(1):172–181, 2018.

[4] Geng-Bo Wu, Shi-Wei Qu, Shiwen Yang, and Chi Hou Chan. Low-cost 1-d beam-steering reflectarray with ±70° scan coverage. *IEEE Transactions on Antennas and Propagation*, 68(6):5009–5014, 2020.

[5] Xue Yang, Shenheng Xu, Fan Yang, Maokun Li, Yangqing Hou, Shuidong Jiang, and Lei Liu. A broadband high-efficiency reconfigurable reflectarray antenna using mechanically rotational elements. *IEEE Transactions on Antennas and Propagation*, 65(8):3959–3966, 2017.

[6] Hirokazu Kamoda, Toru Iwasaki, Jun Tsumochi, Takao Kuki, and Osamu Hashimoto. 60-ghz electronically reconfigurable large reflectarray using single-bit phase shifters. *IEEE Transactions on Antennas and Propagation*, 59(7):2524–2531, 2011.

[7] L. Moustafa, R. Gillard, F. Peris, R. Loison, H. Legay, and E. Girard. The phoenix cell: A new reflectarray cell with large bandwidth and rebirth capabilities. *IEEE Antennas and Wireless Propagation Letters*, 10:71–74, 2011.

[8] Andrea Guarriello, Guillaume Courtin, Renaud Loison, and Raphael Gillard. A general equivalent circuit model for phoenix cells. *IEEE Transactions on Antennas and Propagation*, pages 1–1, 2021.

[9] G. Zhao, Y. Jiao, F. Zhang, and F. Zhang. A subwavelength element for broadband circularly polarized reflectarrays. *IEEE Antennas and Wireless Propagation Letters*, 9:330–333, 2010.

[10] M. Zhou, S. B. Sørensen, O. S. Kim, E. Jørgensen, P. Meincke, O. Breinbjerg, and G. Toso. The generalized direct optimization technique for printed reflectarrays. *IEEE Transactions on Antennas and Propagation*, 62(4):1690–1700, 2014.

[11] H. Legay, D. Bresciani, E. Labiole, R. Chiniard, E. Girard, G. Caille, D. Calas, R. Gillard, and G. Toso. A 1.3 m facetted reflectarray in ku band. In *2012 15 International Symposium on Antenna Technology and Applied Electromagnetics*, pages 1–4, 2012.

[12] J. Fouany, M. Thevenot, E. Arnaud, F. Torres, C. Menudier, T. Monediere, and K. Elis. New concept of telemetry x-band circularly polarized antenna payload for cubesat. *IEEE Antennas and Wireless Propagation Letters*, 16:2987–2991, 2017.

[13] G. Minatti, F. Caminita, E. Martini, M. Sabbadini, and S. Maci. Synthesis of modulated-metasurface antennas with amplitude, phase, and polarization control. *IEEE Transactions on Antennas and Propagation*, 64(9):3907–3919, 2016.

[14] R. Ravanelli, C. Iannicelli, N. Baldecchi, and F. Franchini. Multi-objective optimization of an isoflux antenna for leo satellite down-handling link. In *18-th INTERNATIONAL CONFERENCE ON MICROWAVES, RADAR AND WIRELESS COMMUNICATIONS*, pages 1–4, 2010.

[15] G. Minatti, S. Maci, P. De Vita, A. Freni, and M. Sabbadini. A circularly-polarized isoflux antenna based on anisotropic metasurface. *IEEE Transactions on Antennas and Propagation*, 60(11):4998–5009, 2012.

[16] G. Minatti, M. Faenzi, E. Martini, F. Caminita, P. De Vita, D. González-Ovejero, M. Sabbadini, and S. Maci. Modulated metasurface antennas for space: Synthesis, analysis and realizations. *IEEE Transactions on Antennas and Propagation*, 63(4):1288–1300, 2015.